JOURNAL OF SYNCHROTRON RADIATION
ISSN 1600-5775

Computer simulations of X-ray phase-contrast images and microtomographic observation of tubules in dentin

T. S. Argunova,[a]* V. G. Kohn,[b] J.-H. Lim,[c] Z. V. Gudkina[a,d] and E. D. Nazarova[a,d]

[a]Ioffe Institute RAS, Polytekhnicheskaya St 26, 194021 St Petersburg, Russia, [b]National Research Centre 'Kurchatov Institute', 1 Kurchatov Sq., Moscow, Russia, [c]Pohang Accelerator Laboratory, 80 Jigokro-127-beongil, Namku, Pohang, Republic of Korea, and [d]Faculty of Applied Mathematics and Mechanics, Peter the Great St Petersburg Polytechnic University, Polytekhnicheskaya St 29, St Petersburg, Russia. *Correspondence e-mail: argunova_t@yahoo.com

Received 20 December 2018
Accepted 7 December 2019

Edited by S. M. Heald, Argonne National Laboratory, USA

Keywords: phase-contrast imaging; phase-contrast tomography; computer simulations; dentinal tubules.

An investigation of the problems of X-ray imaging of dentinal tubules is presented. Two main points are addressed. In the first part of this paper, the problem of computer simulating tubule images recorded in a coherent synchrotron radiation (SR) beam has been discussed. A phantom material which involved a two-dimensional lattice of the tubules with parameters similar to those of dentin was considered. By a comparative examination of two approximations, it was found that the method of phase-contrast imaging is valid if the number of tubules along the beam is less than 100. Calculated images from a lattice of 50 × 50 tubules are periodic in free space but depend strongly on the distance between the specimen and the detector. In the second part, SR microtomographic experiments with millimetre-sized dentin samples in a partially coherent beam have been described. Tomograms were reconstructed from experimental projections using a technique for incoherent radiation. The main result of this part is the three-dimensional rendering of the directions of the tubules in a volume of the samples. Generation of the directions is possible because a tomogram shows the positions of the tubules. However, a detailed tubule cross-section structure cannot be restored.

1. Introduction

X-ray tomography has proven to be very powerful in the structural characterization of materials (Baruchel *et al.*, 2000; Stock, 2008). Nowadays, two ways of implementing tomography are available, *i.e.* conventional absorption mode and phase-contrast mode. In absorption mode, tomography has serious limitations in studying micrometre-size objects, *e.g.* cracks, micropipes, tubules and micropores in materials. For a relatively large object, the absorption contrast is strong, while the deflection angles due to refraction at distances of centimetres are very small compared with the object size. Absorption decreases with decreasing object size. At the same time, deflection increases with respect to the object size. For coherent light provided by a third-generation synchrotron radiation (SR) source the increase may come to the point where the image of the micro-object is determined only by the phase. The SR beam should no longer be considered as a parallel beam; hence, strictly speaking, conditions for conventional tomography are not being met.

In order to obtain real-space parameters of a small object, it is necessary to solve the inverse problem. Phase retrieval algorithms combined with tomographic reconstruction techniques have been elaborated for the purpose of obtaining phase data just behind some simple objects (see, for example,

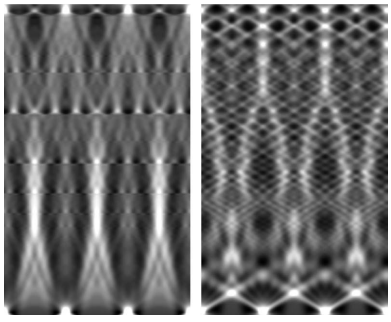

Gureyev *et al.*, 2007; Langer *et al.*, 2008; Vågberg *et al.*, 2015). However, none of commercial programs implement them.

The problem is further complicated by the structure of the object itself. Let us consider two examples of porous media. The first example is an idealized 2D photonic crystal consisting of a square lattice of empty cylinders of diameter 0.5 μm and with a period comparable with the wavelength of visible light. A more complex model, such as that with a slightly disordered lattice of tubules with a section size of 3–5 μm spaced a distance of 10 μm apart, exemplifies the structure of a biocomposite, *e.g.* dentin. Due to their 3D structure, such objects highlight the fact that it is necessary to solve the inverse problem in two dimensions because of a complex refraction–diffraction phenomenon. The refraction of X-rays occurs not only in the rotation plane of a specimen but also in the direction of the rotation axis. Up to now, no such solution has been attempted for the inverse problem. However, a quantitative 3D characterization of porosity is necessary for understanding the unique properties of porous media.

Microporosity within a material can be detected and quantified using in-line imaging techniques (Snigirev *et al.*, 1995; Cloetens *et al.*, 1996). Among the works where in-line images of pores have been investigated with the support of numerical simulations we mention in particular the papers by Agliozzo & Cloetens (2004), Kohn *et al.* (2013), Kohn, Argunova & Je (2014) and Zabler *et al.* (2006). The modeling procedures use standard approximations. In particular, the change in the trajectory of the X-rays within the object is neglected, and the wavefunction acquires a phase shift and a change in amplitude due to changes in the electron density and absorption. The above-cited simulation methods were applied to micrometre-sized porosity in quasicrystals, to a micropipe in a SiC single crystal and to a single tubule in dentin. In a specimen with an array of tubules, which are spaced apart by a distance comparable with their section sizes, the perturbation of the wavefunction occurs all along the specimen. On the other hand, a quasi-periodic distribution of tubules modulates the intensity in free space behind the specimen.

In the first part of this paper, we present and discuss the results of computer simulations of these effects in in-line images of a phantom material similar to dentin. To simplify the simulations, it is assumed that the radiation is coherent and that the specimen has a special orientation, where the tubules are parallel to each other, at least within the first Fresnel zone. In real dentin specimens, the tubules are not straight parallel cylinders.

Knowledge of the tubule orientation is necessary for mechanical, medical and other studies. In particular, the anisotropy of mechanical properties as well as mechanisms of toughening in dentin (Nalla *et al.*, 2003; Kinney *et al.*, 2005; Koester *et al.*, 2008) are due to the effects of dentinal tubules. The directions of these tubules determine the loading geometry used for mechanical testing. In this work, SR microtomography is employed to visualize the tubule network in millimetre-sized dentin samples after uniaxial compression tests.

The second part of the paper presents results of the microtomographic experiments. Projection images that correspond to a given angle of the sample are recorded at a relatively small distance from the sample, where image enlargement can be minimized. The incident radiation is not fully coherent, and the degree of coherence is not measured. None of the projections show interference fringes. This is why conventional absorption microtomography can give reasonable results concerning the visualization of tubules. The reconstruction technique for incoherent radiation produces tomograms showing the positions of the tubules but without sufficient evidence of the tubule cross-section structure. The main result of this part is the generation of the directions of the tubules in a volume of the dentin samples.

2. Computer simulations of phase-contrast images of a model object similar to human dentin

Dentin is a natural porous material with a hierarchical structure. It contains quasi-cylindrical microchannels (herein called tubules) of very low electron density (approximately empty space) of about 3–5 μm diameter. The distance between the tubules is more than two times greater than the tubule diameter. The substance around them has a rather complex structure. Fifty percent of the volume is filled with calcium hydroxyapatite $Ca_5P_3O_{13}H$ of density 3.16 g ccm^{-1}. The rest of the volume is filled with other substances, primarily of collagen fibrils containing only light elements. We believe that they have little effect on the refractive index. As for the evaluation of their contribution, we emphasize that our approach considers a model object that is only approximately similar to a real dentin specimen.

Computer simulations were performed for an X-ray photon energy $E = 12$ keV. The following values of the decrement of the refractive index δ and the absorption index β were used in the calculations: $\delta = 2.26 \times 10^{-6}$, $\beta = 3.62 \times 10^{-8}$. The parameters δ and β were calculated from the chemical composition and half density of calcium hydroxyapatite by means of online programs (Kohn, 2013). We consider a set of cylindrical tubules with diameter $D = 4$ μm and distance $p = 2.5D$ between them. The phase-contrast method assumes that absorption varies weakly inside an object whose thickness variation is relatively small along the beam, *i.e.* the direction parallel to the optical axis. However, the phase shift may be significant, because a thickness variation of only a few micrometres is enough to give a phase shift of the order of π. Due to the fact that the refractive index of a material, *i.e.* $n = 1 - \delta$, deviates slightly from unity, we can assume that the trajectories of the X-rays are not changed. Therefore it is sufficient to calculate the total phase shift of the transmitted X-ray wave on the whole thickness of the object.

In principle, the absorption index can be accumulated on the same trajectory. In this approximation, the perturbation of the wavefunction by the object is described by an exponential factor which is called the transmission function,

$$T(x) = \exp\left\{-i\,\frac{K}{2}\int \mathrm{d}z\,\left[\delta(x,z) - i\beta(x,z)\right]\right\}, \quad K = \frac{2\pi}{\lambda}, \quad (1)$$

where x is the coordinate in the direction normal to the beam direction (z) and the axis of the tubule (y), λ is the wavelength of the X-rays, and the integral is calculated over the whole thickness of the object. The transmission function does not influence the intensity of radiation just behind the object because the phase shift profile is invisible. However, at some sufficiently long distance from the object the phase variation transforms into the intensity variation due to the inhomogeneous density of rays. This is the origin of the phase-contrast technique (Snigirev *et al.*, 1995; Cloetens *et al.*, 1996). To observe a phase-contrast image one has to have coherent radiation and a detector with high spatial resolution, since the mean intensity is not changed.

The approximation (1) can be used with sufficient accuracy for a relatively large object with a size of more than 100 µm, whose thickness slowly varies along the beam. However, dentinal tubules are small, and a dentin specimen may be relatively thick. That is why the accuracy of the approximation (1) must be analyzed. Kohn *et al.* (2018) carried out a detailed analysis of the results of two methods: phase-contrast imaging and a more accurate iterative method developed for studying photonic crystals (Kohn & Tsvigun, 2014; Kohn, Snigireva & Snigirev, 2014). It has been shown that the phase-contrast method based on the transmission function (1) is fairly accurate when applied to specimens containing the number of tubules $N \leq 100$ along the beam. With $N = 200$, the calculated images differ significantly between the two approaches, with only the iterative technique giving an accurate result.

Based on the above analysis, we performed computer simulations of images of a model specimen by means of the phase-contrast technique, where the X-ray wavefunction at the detector is calculated by convolution of the transmission function (2) with the Fresnel propagator $P(x, z)$, namely,

$$\psi(x,z) = \int \mathrm{d}x'\; P(x-x',z)\,T(x')\,P(x-x',z_0), \quad (2)$$

$$P(x,z) = (i\lambda z)^{-1/2}\,\exp\left(i\pi x^2/\lambda z\right), \quad (3)$$

where z_0 is the source-to-object distance and z is the object-to-detector distance. The specimen contained a 2D array of 50×50 tubules in the longitudinal (z) and the transverse (x) directions. The result obtained for an ordered and well oriented lattice of tubules is shown in Fig. 1 (left panel). One can see how the intensity varies in three central periods of 30 µm with the sample-to-detector distance z. The distance has values from 0 to 50 cm. The transverse dimension of the pattern is 20 times smaller than the dimension of the simulation region. We notice that the amplitude of the output wave (at zero distance) is no longer a constant. In the centre of the tubules the amplitude increases by 1.55 times with respect to the area between them. Despite the fact that the change in the phase of the wave is very large, there is also a strong amplitude-contrast associated with absorption.

In the central part of the tubules, the phase change has a parabolic shape, which means that the tubules act on X-rays as micro-lenses. The beams are locally focused at a distance that is slightly less than 1 cm, with a maximum intensity value of 5.5 at the focuses. However, in order to better represent the contrast over the entire range of intensities, the values were trimmed from 0.36 (in the minimum) to 3. An estimation of the focal length (Kohn, 2018) gives a value of 0.88 cm. After focusing, the beams scatter and mix. At some distance interval from 12 to 20 cm, maxima of relative intensity appear between the tubules. With increasing distance, the intensity distribution becomes more uniform, remaining periodic. At a distance of 49 cm, the maxima are formed again close to the centres of the tubules but of lower intensity. Sometimes the intensity behaves in a way that is difficult to understand. The pattern can rapidly rearrange over a short interval of distances or show almost no changes.

It is of interest to model some disorder in the system. Let us consider the same system in which the centre of each new row of tubules has been displaced in the transverse direction randomly relative to the common centre, according to the formula $Up_1(0.5 - R)$, where R is a random number obtained by a random number generator in the interval from 0 to 1. Such a distribution of tubules has one parameter U that can take values from 0 to 1. At $U = 0$ we obtain an ideal lattice; at $U = 1$ we obtain the spread of centres along the entire period.

In the phase-contrast imaging method the phase is summed over all rows along the beam, therefore the periodicity of the distribution remains; however, the profile of the complex phase inside the period can be arbitrarily complicated. Such a system of tubules was generated, and was then used unchanged for different distances. The result of the calculation

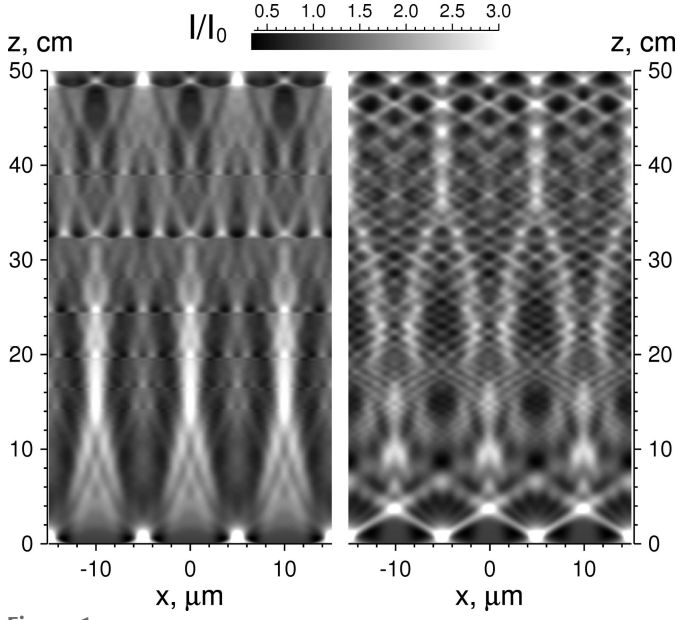

Figure 1
Dependence of the relative intensity of the system, which includes 50×50 tubules of a circular cross-section with a diameter of 4 µm, spaced apart by a distance of 10 µm. Only the central part of the image is shown. Left panel: the structure is a regular lattice. Right panel: the structure contains a weak disorder.

for $U = 0.25$ is shown in Fig. 1 (right panel). It can be seen that even a relatively weak disorder in the system has dramatically changed the intensity distribution in the region behind the focuses. In this case the phase profile is slightly smeared. It deviates somewhat from a parabolic shape, yet focusing occurs. Then, the maxima between the tubules are quickly formed and, starting from a distance of 2 cm, the intensity distribution does not at all resemble the case of the ordered structure.

3. SR phase-contrast tomography experiments

Tomography is a method of computing the attenuation density in 2D sections at a given height of a specimen from experimental images ('projections') that record the integrated attenuation along the X-ray path when the specimen rotates about a vertical axis. A 3D image of the specimen is rendered from 2D sections ('tomograms'). SR tomographic experiments are usually carried out in the near field, *i.e.* at a small distance from the specimen, when there is an unambiguous correspondence between the mutual arrangement of fine structural details in the specimen and their images. Note that, for a bulky specimen with an array of tubules, the images can be distorted by diffraction from the tubules, and solving the inverse problem turns out to be very problematic. The inverse problem has not been solved, and has not intended to be solved in this work. At the same time, the orientation of the tubules is a subject of special interest to us.

Unlike other visualization methods, such as optical or scanning electron microscopy (SEM) (see, for example, Koester *et al.*, 2008; Zaytsev *et al.*, 2014), X-ray tomography is a non-destructive technique, since it does not require chemical etching of dentin. However, tomography is capable of resolving dentinal tubules only under the condition of high spatial resolution. Earlier studies have shown that an X-ray tube with a submicrometre focal spot size offers spatial resolution of 0.2–0.3 μm if the dentin sample size is below $\sim$1 mm^3 (Parkinson & Sasov, 2008). Third-generation SR sources provide instruments that allow a combination of submicrometre spatial resolution and relatively large specimen size.

The experiments were carried out on the 6C wiggler beamline of the Pohang Light Source (PLS), Republic of Korea, operated with full electron energy of 3 GeV. The vertical source size (29 μm) for X-ray energy E = 25 keV (wavelength λ = 0.496 Å) provided a transverse coherence length of 31 μm at the distance 36 m. Phase-contrast images were recorded using a monochromated beam from (111) silicon double-crystal monochromators. A YAG:Ce crystal-scintillator with 30 μm thickness converted X-ray radiation into visible light. The optical objective magnified ($\times$20) and projected the light image on a low-noise 14-bit CCD detector with 0.32 μm effective pixel size. The maximum rendered volume of a specimen had dimensions of 832 μm $\times$ 832 μm $\times$ 702 μm [Fig. 2(*a*)].

Tomographic experiments were performed on crack-free dentin samples after compression tests. For bulk mechanical testing, samples larger than several cubic millimetres are required, but size limitations are imposed by human dentin. Samples of size 3–7 mm^3 were cut using a diamond saw from roots of extracted (caries free) human teeth. A saw-cut was made parallel to the sagittal plane, shown in Fig. 2(*b*) by a dashed line. Samples were flat plates with h = 0.2–0.5 mm thickness [Fig. 2(*c*)]. The damaged layer was removed by abrading the sample surfaces with abrasive paper with a grain size of 10 μm and then by rinsing in clean water. Treatment with acids or other chemicals was excluded.

A series of images ('projections') were recorded as the specimen was rotated about the vertical axis. The projections were taken for each angle $\theta = 0.2°$ between the direction of the X-ray beam and the y axis in the (x, y, z) specimen frame of reference [Fig. 2(*a*)]. The direction of the beam was opposite to the x axis, with z being the axis of rotation. Note that the length l and width w of the specimen are significantly larger

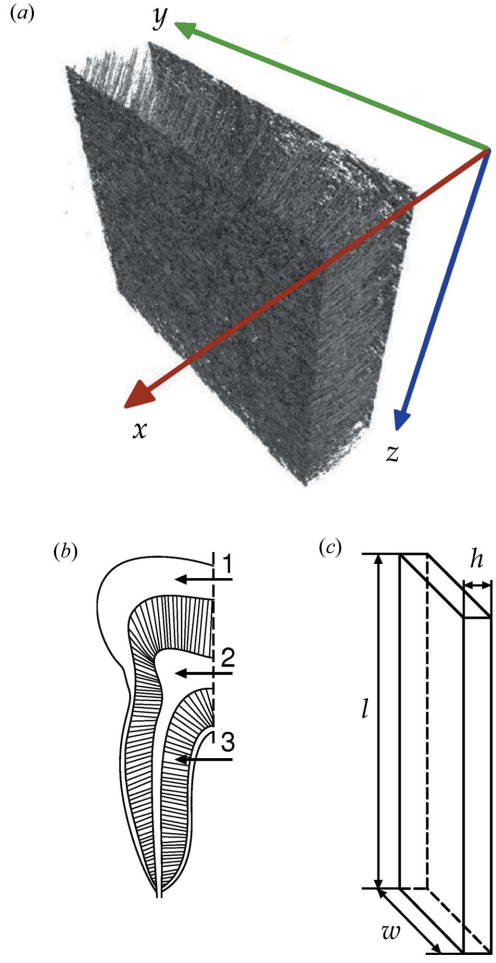

Figure 2
(*a*) 3D rendering of a dentin specimen and its frame of reference. The specimen is in the initial position of rotation, where the beam direction is opposite to the x axis. The rotation axis is parallel to the z axis. A rendered volume of the specimen has dimensions of 832 μm (x) $\times$ 832 μm (y) $\times$ 702 μm (z). (*b*) Sketch of a typical human tooth. 1: enamel; 2: pulp; 3: dentin. The tubules run from the dentin–enamel junction to the pulp. The trace of the sagittal plane is shown by a dashed line. (*c*) Diagram of a dentin specimen used for tomographic experiments after compression tests. Specimen dimensions are typically in the range $\sim$4–5 mm long (l), $\sim$2–3 mm wide (w) and $\sim$0.2–0.5 mm high (h).

than the field of view, which has dimensions of 832 μm (y) × 702 μm (z); but the specimen thickness (h = 200 μm) is less than the dimension 832 μm of the rendered volume in the x direction.

If the size of the beam is not reduced (for instance by setting slits), captured images are formed of a large number of tubules within the specimen. A tubule image increases in size with distance L between specimen and detector. In the case that we considered in the previous section of this paper, the tubule diameter is D = 4 μm and the spacing between their centres is p = 10 μm. If the distance L = 5 cm, then the diameter of the first Fresnel zone $2r = 2(\lambda L)^{1/2}$ = 3.2 μm, *i.e.* less than D, where λ = 0.496 Å. The near-field conditions are met and the tubules may be expected to produce separate images. Nevertheless, the situation changes immediately we take into account only voids with a diameter of 1–2 μm in the sheaths of peritubular dentin (see, for example, Zabler *et al.*, 2006; Imbeni *et al.*, 2003). In this case, the transition from the Fresnel diffraction to the far-field regime begins very close to the sample. This means that a detailed structure of the tubules cannot be obtained.

On experimental projections, tubule contrast always looks like frequently alternating non-periodic stripes. The left-hand panel in Fig. 3 represents images which are not explicable in terms of absorption contrast from spaced cylinders. The most striking feature, however, is that this 'striped' pattern indicates the directions of the tubules. On the reconstructed tomograms, *i.e.* sections (x, y) along the vertical axis z, spots are formed due to increase in intensity. As seen in Fig. 3(b), each spot has a light centre surrounded by a halo with a lower contrast. These signs indicate the interference nature of the tubules images. Absorption contrast alone is not enough to explain the visibility of the tubule cross-sections. This interpretation is supported by available data (Zabler *et al.*, 2006; Zaslansky *et al.*, 2010) that show similar image attributes.

Octopus V8.7 sofware (XrayLAB, Ghent University, Belgium), which has been employed for the reconstruction of the tomograms, takes account of the relative positions of the tubules quite correctly. This follows, in particular, from a comparison of experimental projections and tomograms. Fig. 3(a) shows a projection image of the dentin specimen cut out from the root part of a tooth roughly parallel to a sagittal plane [Fig. 2(b)]. The imaged specimen shows that the tubules lay obliquely to the transverse (x, y) plane. In the other specimen [Fig. 3(c)], the inclination angle is even smaller. A marked decrease in the angle distorts and elongates the spots on corresponding tomograms [Fig. 3(d)]. The elongated spots reflect local changes of the cross sections of the tubules. We note that their density does not show a typical tubule density of 1×10^6 to 1×10^7 cm^2 (Parkinson & Sasov, 2008; Macpherson *et al.*, 1995). This again suggests the occurrence of interferences which results in the tubule cross sections being invisible due to the interference patterns cancelling each other out.

Interesting fan-shaped contrast is apparent on the projection image of the third specimen [Fig. 3(e)], where the fan head is seen at the bottom of the image. On the corresponding tomogram [Fig. 3(f)] a denser distribution of the spots can be attributed to the fan head. Note that the changes in the tubule density are not visible on the projection image [Fig. 3(e)].

In previous investigations, virtual slices from reconstructed 3D data were employed to determine the directions of the tubules. For instance, Zaslansky *et al.* (2010) studied the orientations of tubules in relation to enamel. Virtual images of the tubules were co-aligned and the average tubule orientation was determined. We note that dentinal tubules may look straight and parallel to each other as shown by optical microscopy and ptychography data (Zaytsev *et al.*, 2011; Zanette *et al.*, 2015) as well as by numerous SEM images obtained with fields of view of several tens of micrometres. We also note that the above approach (see Section 2) assumes that the tubules are straight within a length of several micrometres, which corresponds to the first Fresnel zone. Real dentinal tubules are, however, neither straight nor parallel to each other.

On the one hand, projections recorded at various distances between the specimen and the detector show a striped pattern that does not provide any information about the positions of

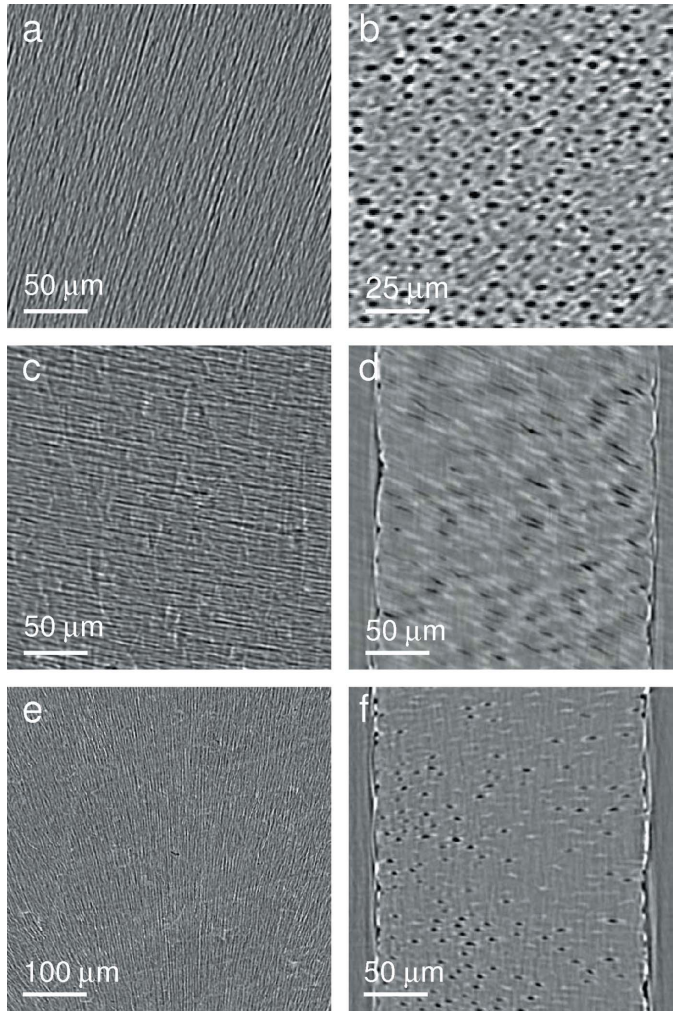

Figure 3
(*a*, *c*, *e*) Fragments of experimental images ('projections'). Tomograms (*b*, *d*, *f*) were reconstructed from these projections, respectively.

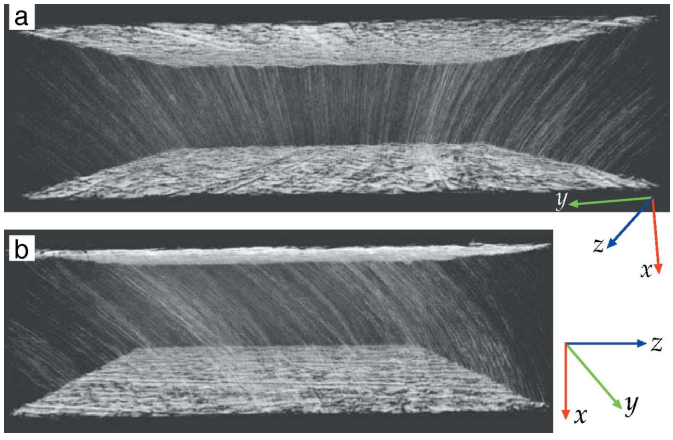

Figure 4
Volume rendering of the dentin specimen, which shows the directions of the tubules. The specimen is viewed along the z axis (a) and the y axis (b).

the tubule centres. On the other hand, tomograms show cross sections of the tubules. We still cannot recognize the orientation of the tubules until we obtain a 3D image of the specimen. Virtual objects have been visualized using *Amira* V6.0 software (Visage Imaging GmbH, Germany). Fig. 4 shows volume rendering of the dentin specimen shown in Figs. 3(e) and 3(f). The lines visible in Fig. 4 represent the directions of the tubules in 3D space. The distribution of the lines is rather complex. They reveal neither the size nor the shape of the tubules themselves, but orientation of the tubules can be quite useful for various applications.

4. Summary

Computer simulations of phase-contrast images of a model object were performed. The object was composed of the lattice of tubules that were about the same size and spacing as dentinal tubules. Calculated images of the object in a coherent SR beam depend strongly on the distance between the object and the detector. The images show that the period of the lattice can be determined.

Dentin samples were prepared as millimetre-sized plates without acid treatment. Experiments with X-ray microtomography in a partially coherent SR beam were performed. Images ('projections') were recorded at a small distance between the sample and the detector. Oriented black and white stripes are a specific image contrast characteristic of dentin samples in general. The 'striped' contrast pattern does not correspond to the positions of the tubules in the specimen and does not resemble interference fringes. The pattern, however, indicates the directions of the tubules.

Tomograms (2D slices at a given sample height) were reconstructed using an algorithm and software for incoherent radiation. On the tomograms, the tubules produce spot-like areas of inhomogeneous contrast enhancement. 3D volume rendering of a dentin sample shows lines that represent the directions of the tubules, but the tubule cross-section structure cannot be restored.

A future challenge will be to explain the formation of the tubule contrast. Comparison of experimental and simulated tomograms should help to find out the main causes of distortions in the line shapes, when the rotation of the sample makes a tubule wiggle about. The interference nature of the contrast can be elucidated through the reconstruction of tomograms from projections recorded at various specimen-to-detector distances. Other techniques, such as optical microscopy or SEM, should be used to determine the range of tubule diameters.

References

Agliozzo, S. & Cloetens, P. (2004). *J. Microsc.* **216**, 62–69.
Baruchel, J., Buffiere, J. Y. & Maire, E. (2000). *X-ray Tomography in Material Science.* Paris: Hermes Science Publications.
Cloetens, P., Barrett, R., Baruchel, J., Guigay, J.-P. & Schlenker, M. (1996). *J. Phys. D Appl. Phys.* **29**, 133–146.
Gureyev, T. E., Nesterets, Ya. I. & Mayo, S. C. (2007). *Opt. Commun.* **280**, 39–48.
Imbeni, V., Nalla, R. K., Bosi, C., Kinney, J. H. & Ritchie, R. O. (2003). *J. Biomed. Mater. Res.* **66A**, 1–9.
Kinney, J. H., Nalla, R. K., Pople, J. A., Breunig, T. M. & Ritchie, R. O. (2005). *Biomaterials*, **26**, 3363–3376.
Koester, K. J., Ager, J. W. III & Ritchie, R. O. (2008). *Biomaterials*, **29**, 1318–1328.
Kohn, V. G. (2013). *Refraction index*, http://kohnvict.ucoz.ru/jsp/2-irpar.htm.
Kohn, V. G. (2018). *J. Synchrotron Rad.* **25**, 425–431.
Kohn, V. G., Argunova, T. S. & Je, J. H. (2013). *AIP Adv.* **3**, 122109.
Kohn, V. G., Argunova, T. S. & Je, J. H. (2014). *AIP Adv.* **4**, 097134.
Kohn, V. G., Argunova, T. S. & Je, J. H. (2018). *Phys. Status Solidi B*, **255**, 1800209.
Kohn, V. G., Snigireva, I. & Snigirev, A. (2014). *J. Synchrotron Rad.* **21**, 729–735.
Kohn, V. G. & Tsvigun, N. V. (2014). *Crystallogr. Rep.* **59**, 1–5.
Langer, M., Cloetens, P., Guigay, J.-P. & Peyrin, F. (2008). *Med. Phys.* **35**, 4556–4566.
Macpherson, J. V., Beeston, M. A., Unwin, P. R., Hughes, N. P. & Littlewood, D. (1995). *Langmuir*, **11**, 3959–3963.
Nalla, R. K., Kinney, J. H. & Ritchie, R. O. (2003). *Biomaterials*, **24**, 3955–3968.
Parkinson, C. R. & Sasov, A. (2008). *Dent. Mater.* **24**, 773–777.
Snigirev, A., Snigireva, I., Kohn, V., Kuznetsov, S. & Schelokov, I. (1995). *Rev. Sci. Instrum.* **66**, 5486–5492.
Stock, S. R. (2008). *Int. Mater. Rev.* **53**, 129–181.
Vågberg, W., Larsson, D. H., Li, M., Arner, A. & Hertz, H. M. (2015). *Sci. Rep.* **5**, 16625.
Zabler, S., Riesemeier, H., Fratzl, P. & Zaslansky, P. (2006). *Opt. Express*, **14**, 8584–8597.
Zanette, I., Enders, B., Dierolf, M., Thibault, P., Gradl, R., Diaz, A., Guizar-Sicairos, M., Menzel, A., Pfeiffer, F. & Zaslansky, P. (2015). *Sci. Rep.* **5**, 9210.
Zaslansky, P., Zabler, S. & Fratzl, P. (2010). *Dent. Mater.* **26**, e1–10.
Zaytsev, D., Grigoriev, S. & Panfilov, P. (2011). *Mater. Lett.* **65**, 2435–2438.
Zaytsev, D., Ivashov, A. S., Mandra, J. V. & Panfilov, P. (2014). *Mater. Sci. Eng. C*, **41**, 83–90.